Supplementary materials for

Fingerprinting the source and complex history of ore fluids of lode gold deposits using quartz textures and in-situ oxygen isotopes

Gao-Hua Fan[1, 2], Jian-Wei Li[1, 2*], Ya-Fei Wu[2], Xiao-Dong Deng[1], Fang-Yue Wang[3], Wen-Sheng Gao[2], Si-Yuan Li[2], Liang Fan[2]

[1] State Key Laboratory of Geological Process and Mineral Resources, China University of Geosciences, Wuhan 430074, China

[2] School of Earth Resources, China University of Geosciences, Wuhan 430074, China

[3] Ore Deposit and Exploration Centre (ODEC), School of Resources and Environmental Engineering, Hefei University of Technology, Hefei 230009, China

Corresponding author:

e-mail: jwli@cug.edu.cn

Tel: +0086-27-67883563

1. The calculation of $\delta^{18}O$ values of quartz-forming aqueous fluids

The $\delta^{18}O_{water}$ values were evaluated based on the quartz-water fractionation equation of Fekete et al. (2016).

$$\Delta^{18}O_{phase1 - phase2} \approx 1000ln_{1-2} = A_{1-2} \times 10^6/T^2 + B_{1-2} \times 10^3/T + C_{1-2} \qquad (1)$$

Where T is the temperature in Kelvin. A = 3.3308, B = 0, C = –2.7734.

2. The effects of different fluid processes on $\delta^{18}O_{water}$ variations

2.1. Fluid-rock interaction

Fluid-rock interaction involving oxygen isotope exchange between magmatic fluid (assumed $\delta^{18}O_{water} \approx 7.5‰$ representing herein the maximum $\delta^{18}O_{water}$ value) and the ore-hosting syenite (average $\delta^{18}O = 7.1‰$; Zhang, 1996) in closed and open systems were modelled based on the following equations of Taylor (1977).

Closed systems:

$$\delta^{18}O_{f.\ water} = [\delta^{18}O_{i.\ rock} + (W/R) \times \delta^{18}O_{i.\ water} - \Delta^{18}O_{rock-water}] / [1 + (W/R)] \qquad (2)$$

Where W = atom per cent of the oxygen isotope in hydrothermal fluid, R = atom per cent of the oxygen isotope in the rock, $\delta^{18}O_{i.}$ and $\delta^{18}O_{f.}$ are the initial and final oxygen isotopic compositions, respectively, of the rock and fluid involved in the isotopic exchange reactions. The $\Delta^{18}O_{rock-water}$ is the temperature-dependent rock-fluid relative isotopic fractionation. For granitic rocks (represented here by the syenite), $\delta^{18}O_{f.\ rock}$ is usually equal to the $\delta^{18}O$ value of plagioclase (An$_{30}$) (Taylor, 1977), thus the feldspar-water geothermometer can be used to calculate $\Delta^{18}O_{rock-water}$ at any temperature ($1000ln\alpha = 2.68 \times (10^6 / T^2) -3.29$, where the T is the temperature in Kelvin) (Taylor, 1986).

Open systems:

$$(W/R)_{\text{open system}} = \ln \left[(W/R)_{\text{closed system}} + 1 \right] \tag{3}$$

2.2. Rayleigh distillation

The isotopic composition of hydrothermal fluid can be progressively modified by the precipitation of mineral due to isotope fractionation between mineral and fluid. Here, we modelled the oxygen isotope fractionation between quartz and magmatic fluid in such system using Rayleigh fractionation equation:

$$R_{\text{f. water}} / R_{\text{i. water}} = F^{(\alpha_{\text{water}}^{\text{mineral}}-1)} \tag{7}$$

Where R_i and R_f are the isotopic ratios of initial and final fluid, respectively. F is the fraction of the element remaining in the fluid, and α is the temperature-dependent isotope fractionation factor of the element considered between mineral and fluid.

Substituting the isotope ratios using delta values from the following equation:

$$\delta = 1000 \times \left[(R/R_{\text{std}}) - 1 \right] \tag{8}$$

Then, equation (4) can be rewritten as:

$$\ln \left[(1000+\delta_{\text{f. water}}) / (1000+\delta_{\text{i. water}}) \right] = (\alpha_{\text{water}}^{\text{mineral}}-1) \times \ln F \tag{9}$$

By rearranging equation (6) using the following approximation equation:

$$\ln \left[(1000+\delta_{\text{f. water}}) / (1000+\delta_{\text{i. water}}) \right] \approx (\delta_{\text{f. water}} - \delta_{\text{i. water}}) / 1000 \tag{10}$$

Finally, an expression can be obtained for $\delta_{\text{f. water}}$:

$$\delta_{\text{f. water}} = \delta_{\text{i. water}} + 1000 \times (\alpha_{\text{water}}^{\text{mineral}}-1) \times \ln F \tag{11}$$

2.3. Fluid mixing

The proportions (A) of meteoric water during the formation of quartz veins of various stages at Dongping can be estimated based on the isotopic mass balance between

meteoric water (average $\delta^{18}O = -12.5$‰; Zhang, 1996; Zha, 2020) and magmatic fluid:

$$\delta^{18}O_{f.\ water} = A \times \delta^{18}O_{meteoric\ water} + (1 - A) \times \delta^{18}O_{magmatic\ fluid} \qquad (12)$$

The highest $\delta^{18}O_{water}$ for quartz at Dongping is 7.5‰, which can be used to calculate the minimum A. The $\delta^{18}O$ values of magmatic fluids range from 10 to 5‰, thus, the $\delta^{18}O_{water}$ value of 10‰ can be assumed to calculate the maximum A.
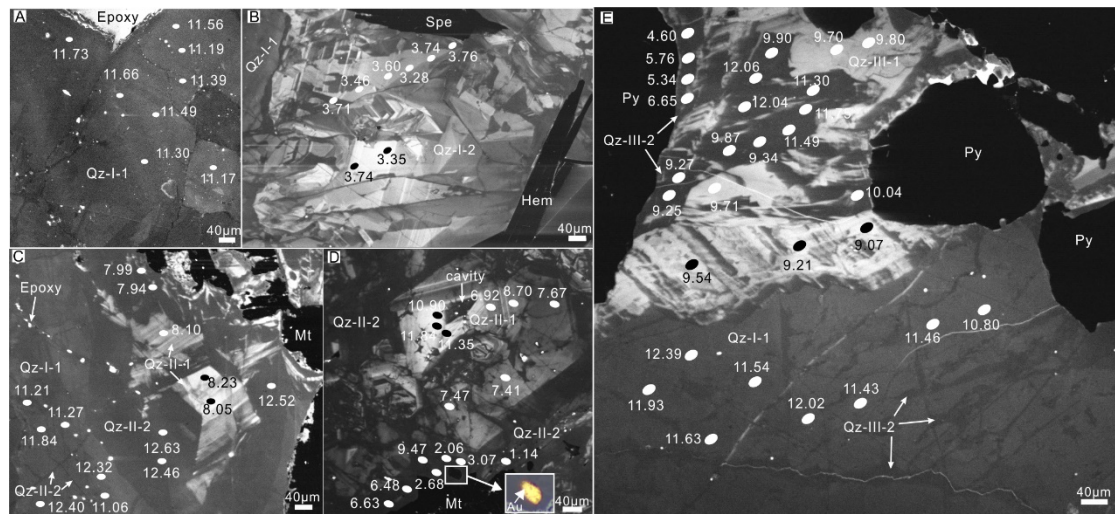
Figure S1

Figure S1. SEM-CL images showing textures of various quartz generations. White ellipses represent the locations of *in-situ* $\delta^{18}O$ analysis pits. A. White quartz (Qz-I-1) of stage I showing mottled to homogeneous texture. B. Gray quartz (Qz-I-2) of stage I replaced the pre-existing Qz-I-1 and shows a mosaic texture with heterogeneous CL intensities. Specularite is intergrown with Qz-I-2. C–D. Gray quartz of stage II consists of Qz-II-1 and Qz-II-2. Zoned Qz-II-1 is usually overprinted or replaced by late homogeneous CL-dark Qz-II-2, which also occurs as veinlets invading into the white quartz (Qz-I-1) of stage I. E. Gray quartz of stage III is composed of Qz-III-1 and Qz-III-2, which show homogeneous CL-bright and CL-dark texture, respectively. Qz-III-2 replaced or crosscut the white quartz (Qz-I-1) of stage I and Qz-III-1. Mt = magnetite, Spe = specularite, Py = pyrite.
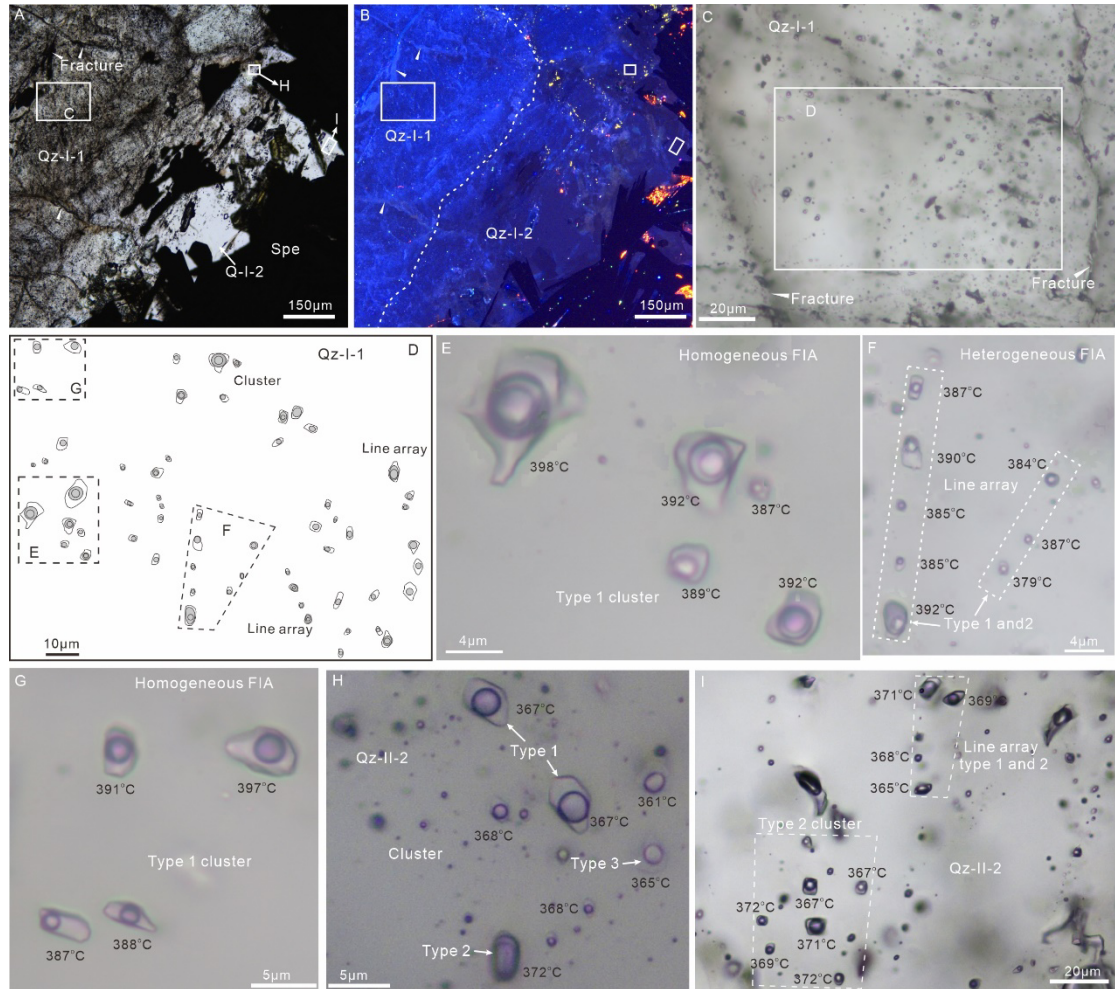
Figure S2

Figure S2. Photomicrographs under transmitted light (A, C–I) and OM-CL images (B)

showing texture of Qz-I-1 and Qz-I-2 of stage I, and occurrence of fluid inclusion types

in these two generations. A. Transmitted light image shows that gray quartz (Qz-I-2) of

stage I is more transparent relative to white quartz (Qz-I-1). Specularite is intergrown

with Qz-I-2. Some microfractures are also clear in Qz-I-1. B. OM-CL image shows that

Qz-I-1 and Qz-I-2 are homogeneously bright and dark blue, respectively. Whtie

triangles denote the microfractures. Different textures of Qz-I-2 revealed by OM- and

SEM-CL images are due to the different luminescence principles of quartz under the

operating conditions of these two techniques (Götze and Kempe, 2008). C–I.

Representative high-magnification area outlined in Fig. S2A showing the occurrence

and distribution of homogeneous- and heterogeneous-trapping FIAs in Qz-I-1 (C–G)

and Qz-I-2 (H, I). These FIAs usually occur as random clusters and/or line arrays.

Temperatures close to FI represent the final homogeneous temperatures.
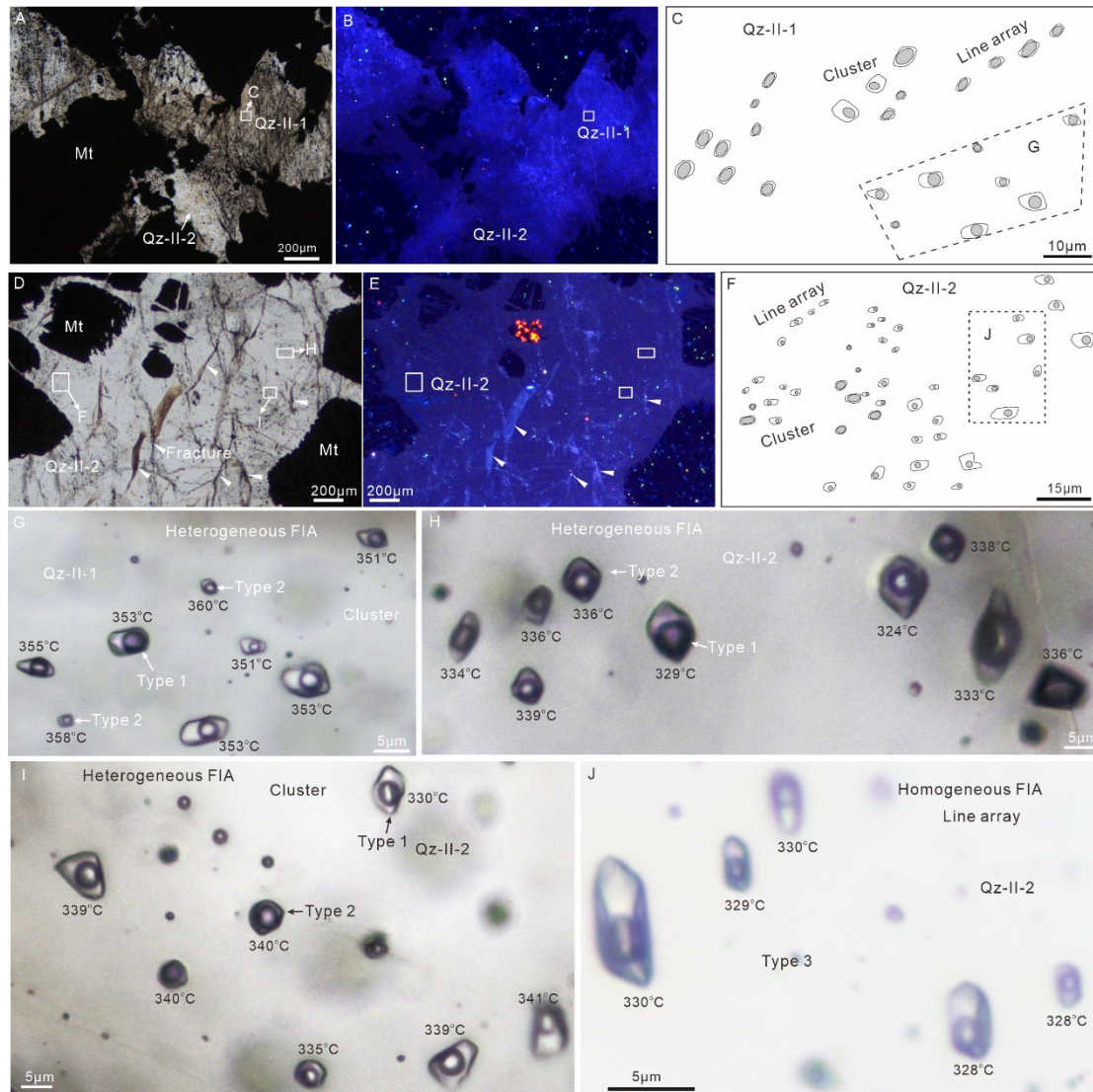
Figure S3

Figure S3. Photomicrographs showing the textural characteristics and occurrence of fluid inclusion in Qz-II-1 and Qz-II-2 identified in gray quartz of stage II. Qz-II-2 is more transparent relative to Qz-II-1 (A, D). OM-CL images show that Qz-II-1 shows a homogeneity in OM-CL intensity (B) different from the zoning texture shown in SEM-CL images, whereas Qz-II-2 shows a homogeneous CL-dark texture (B, E) similar to SEM-CL texture. C, F–G. Representative high-magnification area outlined in Fig. S3A and D showing the occurrence and distribution of homogeneous- and heterogeneous-trapping FIAs in Qz-II-1 (C, G) and Qz-II-2 (F, H–J). These FIAs usually occur as

random clusters and/or line arrays. Temperatures close to FI denote the final
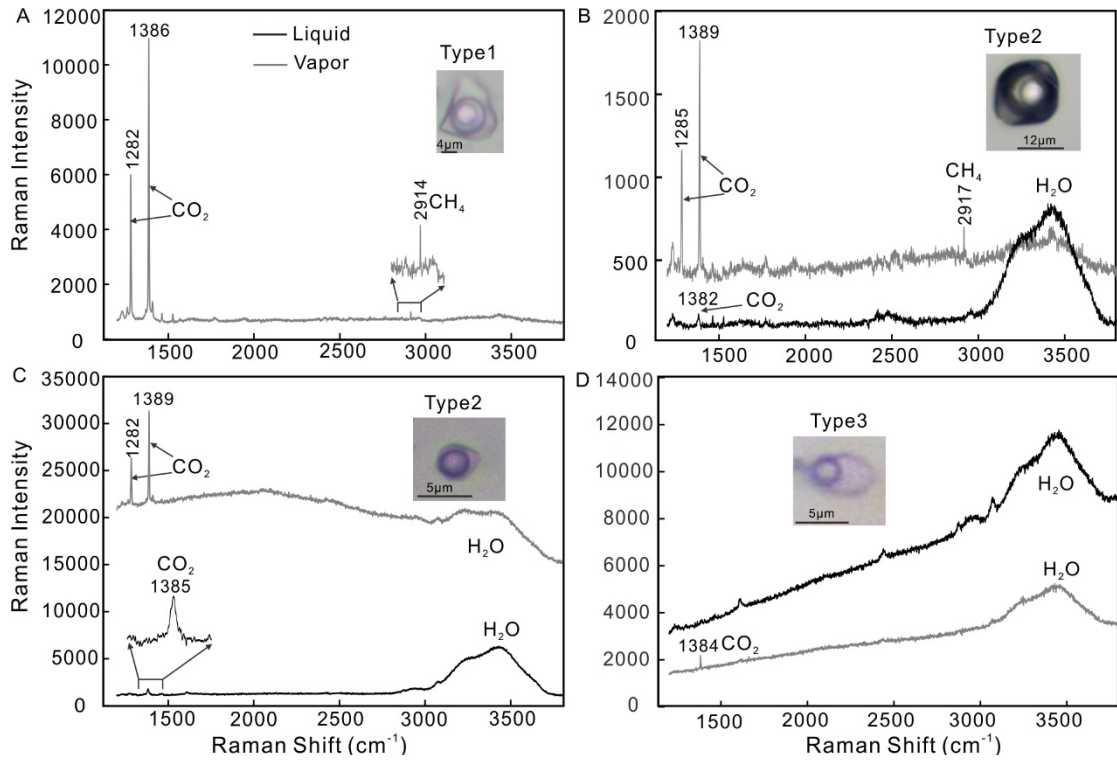
homogeneous temperatures.

Figure S4

Figure S4. Raman spectrum of aqueous-carbonic (type 1, 2) and aqueous-dominated (type 3) inclusions. A. Aqueous-carbonic inclusions (type 1) consist predominantly of CO_2 with trace amounts of CH_4. B–C. Vapor phase of aqueous-carbonic inclusions (type 2) is mainly composed of CO_2 with minor CH_4, whereas liquid phase is dominated by H_2O with minor CO_2. D. Both vapor and liquid phases of type 3 inclusions are dominated by H_2O, but minor CO_2 is also present in vapor phase.

References

Fekete, S., Weis P., Driesner, T., Bouvier, A. S., Baumgartner, L., Heinrich, C. A., 2016. Contrasting hydrological processes of meteoric water incursion during magmatic–hydrothermal ore deposition: an oxygen isotope study by ion microprobe. Earth Planet. Sci. Lett. 451, 263–271.

Götze, J., Kempe, U., 2008. A comparison of optical microscope-and scanning electron microscope-based cathodoluminescence (CL) imaging and spectroscopy applied to geosciences. Mineral. Mag. 72, 909–924.

Taylor, E., 1986. Magmatic volatiles; isotopic variation of C. H, and S. Rev. Mineral. 16, 185–225.

Taylor, H. P., 1977. Water/rock interactions and the origin of H_2O in granitic batholiths. J. Geol. Soc. Lond. 133, 509–558.

Zhang, Z. C., 1996. Characteristics of H and O isotopes and fluid evolution in Dongping gold deposit. Gold Geol. 30, 36–41.

Zha, Z. J., 2020. Geological and geochemical characteristics and genesis of the Zhongshangou gold deposit in northwest Hebei Province. M.S. thesis, China University of Geosciences, Beijing, p. 54–56.